

Linear scaling causal discovery from high-dimensional time series by dynamical community detection

Matteo Allione,^{1,*} Vittorio Del Tatto,^{1,*} and Alessandro Laio^{1,2,†}

¹*Scuola Internazionale Superiore di Studi Avanzati (SISSA), via Bonomea 265, 34136 Trieste, Italy*

²*International Centre for Theoretical Physics (ICTP), Trieste 34151, Italy*

Understanding which parts of a dynamical system cause each other is extremely relevant in fundamental and applied sciences. However, inferring causal links from observational data, namely without direct manipulations of the system, is still computationally challenging, especially if the data are high-dimensional. In this study we introduce a framework for constructing causal graphs from high-dimensional time series, whose computational cost scales linearly with the number of variables. The approach is based on the automatic identification of *dynamical communities*, groups of variables which mutually influence each other and can therefore be described as a single node in a causal graph. These communities are efficiently identified by optimizing the Information Imbalance, a statistical quantity that assigns a weight to each putative causal variable based on its information content relative to a target variable. The communities are then ordered starting from the fully autonomous ones, whose evolution is independent from all the others, to those that are progressively dependent on other communities, building in this manner a community causal graph. We demonstrate the computational efficiency and the accuracy of our approach on time-discrete and time-continuous dynamical systems including up to 80 variables.

Introduction — The growing abundance of time series - spanning fields from environmental monitoring to finance and neuroscience - offers unprecedented opportunities for understanding real world observations. Specifically, causal discovery allows studying how different parts of a system influence each other and inferring the existence of directional couplings (or causal relationships) between variables in a time series [1–3]. The results of such analysis can reveal how the effects of an external intervention spread throughout the system and can help to construct parsimonious models that describe physical relationships with a reduced number of parameters [4].

Relationships between variables can be depicted, using Pearl’s approach [5, 6], as a time series graph. Each dynamic variable at a specific time is represented by a node and an arrow from one node to another represents a direct causal link. Such a graph encodes all conditional independence relationships between pairs of variables [2, 7, 8]. Several strategies can be used to build this graph. A first option involves checking for each couple of lagged variables if there is no conditioning set that makes them independent. An arrow between the two nodes is then drawn only if there is no such set [9]. A strategy to assess the existence of such a conditioning set is to employ an iterative approach, where the size of the tested set is progressively increased [10, 11]. Although this approach leads to optimal detection power, namely to a small rate of false negatives, it requires performing a number of tests that scales exponentially with the number of variables. Therefore strategies to reduce the search space in practical applications have been developed [12, 13]. Alternatively, one can directly consider for each pair of lagged variables the

largest possible conditioning set, which includes all past history of the time series. The multivariate versions of Granger Causality [14–16] and Transfer Entropy [17] can be regarded as implementations of this second strategy [2, 9]. Although this approach drastically reduces the number of tests to be performed, requiring a single test per pair of variables, it is significantly affected by the curse of dimensionality, often resulting in reduced detection power [12].

In this work, we introduce a method for causal discovery designed for high-dimensional time series. A powerful feature of our approach is that it enables the identification of causal influences that emerge from the collective dynamics of multiple variables at a very moderate computational cost, which, importantly, scales linearly with the number of variables. The graph obtained with our algorithm is a “mesoscopic” version of the standard graphs, as it groups together variables whose evolution cannot be described independently. We call these groups of variables *dynamical communities*. Our approach aims at revealing, if present, a hierarchical organization of these communities. We refer to the resulting graph as *community causal graph*. The key ingredient in this approach is the efficient identification of the dynamical communities. This is achieved by optimizing the Information Imbalance [18, 19] as a function of a set of variational weights, one for each variable of the system. We will show that the values of the weights allow identifying very efficiently the communities and, as a consequence, building a causal graph, avoiding inefficient combinatorial searches of conditioning sets. Our method assumes causal sufficiency, namely that there are no unobserved common drivers of two or more dynamic variables. We demonstrate its effectiveness using time series generated from both discrete-time and continuous dynamical systems, showcasing its applicability to high-dimensional scenarios.

The algorithm exploits the Information Imbalance [18],

* These two authors contributed equally to this work.

† Contact author: laio@sissa.it

which allows quantifying the information content of different distance measures defined on a data set, which we briefly review in the following. The underlying idea is that a distance measure d^A is predictive with respect to another distance measure d^B if points close according to d_A are also close according to d^B . The Information Imbalance is defined as

$$\Delta(d^A \rightarrow d^B) = \frac{2}{N^2} \sum_{\substack{i,j \\ (i \neq j)}} \delta_{r_{ij}^A, 1} r_{ij}^B, \quad (1)$$

where N is the number of points in the dataset, δ is the Kronecker delta and $r_{ij}^{(\cdot)}$ is the rank obtained after sorting in ascending order the pairwise distances between i and rest of the points. The superscript in the ranks refers to the space in which the distances are computed. For example, $r_{ij}^A = 2$ if j is the second nearest neighbor of i according to distance d^A . Eq. (1) defines a quantity that, in the limit of large N , approaches zero when all nearest neighbors in space A remain nearest neighbors in space B , namely when d^A is maximally predictive of d^B .

In ref. [20] we showed that the Information Imbalance can be used to infer the presence of causality between two multidimensional dynamical systems X and Y , under the assumption of causal sufficiency. Adapting the predictability principle of Granger causality [14] to our framework, we assumed that if X causes Y and one attempts to make a prediction of the future of Y , a distance measure built using the present states of both X and Y will have more predictive power than a distance built using only Y . Formally, we assumed that X causes Y if and only if

$$\hat{w} = \underset{w}{\operatorname{argmin}} \Delta(d^{wX(0), Y(0)} \rightarrow d^{Y(\tau)}) \neq 0 \quad (2)$$

for some positive time lag τ . In Eq. (2) and in the following, the notation $d^{(\cdot)}$ denotes the squared Euclidean distance built over the superscript variables. For example,

$$d_{ij}^{wX(0), Y(0)} = w^2 \|X_i(0) - X_j(0)\|^2 + \|Y_i(0) - Y_j(0)\|^2, \quad (3)$$

where the Latin letters i and j denote independent realizations of the same dynamics, which can be either obtained from uncorrelated samples of a single stationary trajectory, or from distinct trajectories with independent initial conditions. Since such distances are invariant under a change of sign of w , we can consider only positive weights. In the Supplemental Material (SM) we relate the criterion in Eq. (2) to the notion of conditional independence commonly employed in causal inference and causal network reconstruction. Importantly, the approach in ref. [20] builds on prior knowledge of the groups of variables that make up the distinct dynamical systems interacting with each other (the dynamical communities in the language of this work, see below). This is a very strong assumption, which for real-world data is

typically violated. This work is dedicated to overcoming this problem.

Here, we extend the approach described above to automatically and efficiently find those dynamical communities. Our algorithm makes use of a differentiable extension of the Information Imbalance (DII) recently introduced by Wild *et al.* [19]:

$$\text{DII}(d^A \rightarrow d^B) = \frac{2}{N^2} \sum_{\substack{i,j \\ (i \neq j)}} \frac{e^{-d_{ij}^A/\lambda}}{\sum_{m(\neq i)} e^{-d_{im}^A/\lambda}} r_{ij}^B. \quad (4)$$

We note that Eq.(4) tends to Eq. (1) in the limit $\lambda \rightarrow 0$. If distance d^A depends on a set of parameters \mathbf{w} , this formulation allows optimizing such parameters by gradient descent.

Our algorithm, illustrated in Fig. 1, can be conceptually divided into three parts: in part i), the DII is iteratively minimized to infer the *autonomous sets*, namely the set of all variables directly or indirectly causing each variable; in part ii), the autonomous sets are used to find the dynamical communities, namely sets of variables which directly or indirectly influence each other; and in part iii), a macroscopic graph depicting the causal interactions between the communities is constructed.

i) Identification of autonomous sets — As a first step we infer the *autonomous set* \mathcal{S}^β of each variable X^β , which we define as the set of all variables $\{X^\alpha\}$ directly or indirectly causing X^β . X^α is a direct cause of X^β if, for some time lag τ , there exists a direct link $X^\alpha(0) \rightarrow X^\beta(\tau)$ in the ground-truth time series graph. Conversely, X^α is an indirect cause of X^β if, for any $\tau > 0$, the only directed path connecting $X^\alpha(0)$ and $X^\beta(\tau)$ pass through at least a third variable $X^\gamma(\tau')$, where $\gamma \neq \alpha$, $\gamma \neq \beta$ and $0 < \tau' < \tau$. In the following, we will use the notations $X^\alpha \rightarrow X^\beta$ and $X^\alpha \in \mathcal{S}^\beta$ interchangeably, without distinguishing between direct and indirect links.

To identify the autonomous sets \mathcal{S}^β , we optimize the Information Imbalance of Eq. (4) between a distance measure built with all dynamic variables at time $t = 0$ and a distance built with a single variable X^β at time $t = \tau$. To level out the fluctuation ranges of different variables, we first scale each variable by its standard deviation over the entire trajectory. Thus, the weights obtained by this optimization are

$$\hat{\mathbf{w}}_\beta = \underset{\mathbf{w}}{\operatorname{argmin}} \text{DII}\left(d^{w \odot \mathbf{X}(0)} \rightarrow d^{X^\beta(\tau)}\right), \quad (5)$$

where \odot denotes the element-wise product. We generalize the principle of Eq. (2) by stating that X^α is a direct or indirect cause of X^β when the α -component of $\hat{\mathbf{w}}_\beta$, denoted by \hat{w}_β^α , is nonzero.

We repeat the optimization in Eq. (5) for several values of τ between 1 and τ_{\max} , where τ_{\max} is a hyper parameter which, in applications, we take of the order of the autocorrelation time of X^β . As depicted in Fig. 1, the

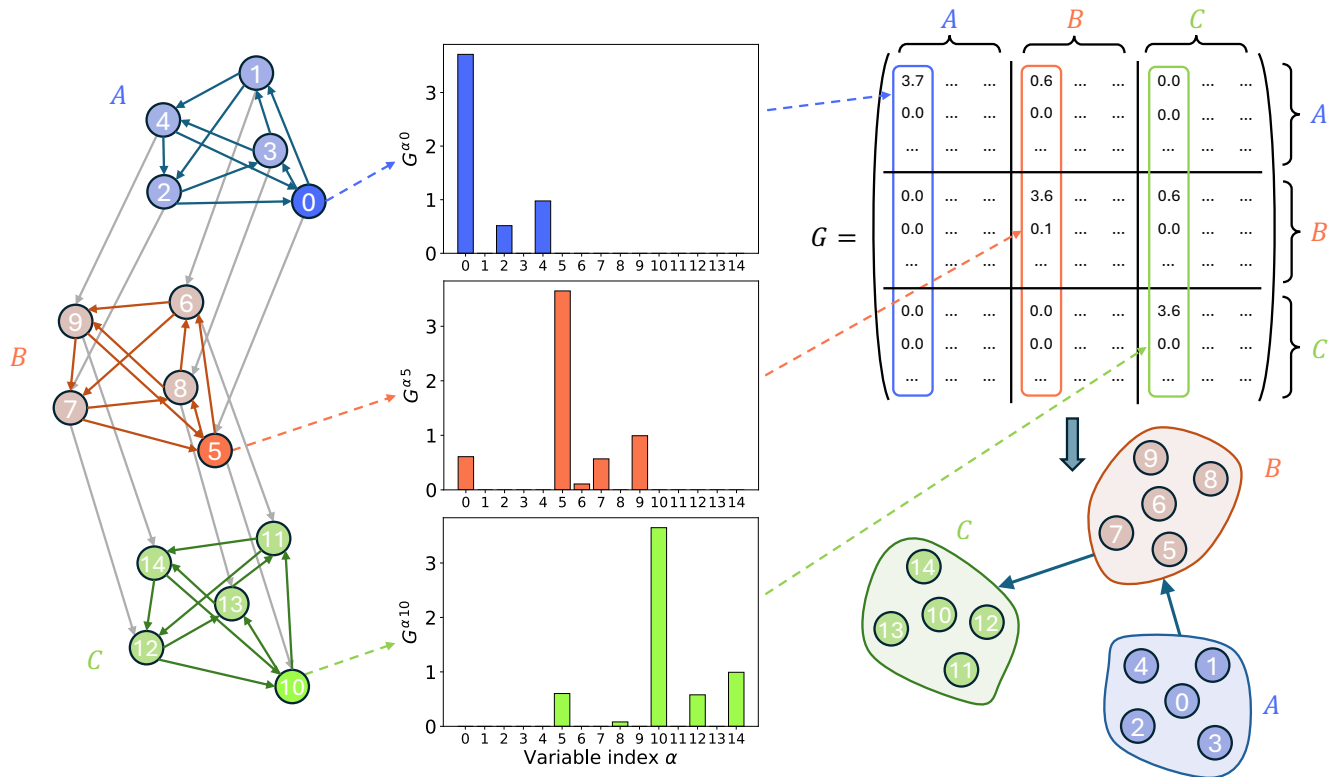


FIG. 1. Illustration of the algorithm, using a 15-dimensional dynamical system composed of three groups of noisy coupled logistic maps. On the left, the ground-truth connectivity of the system is depicted in an all-variable representation. Repeated optimizations of $\text{DII}(d^{\mathbf{w} \odot \mathbf{X}^{(0)}} \rightarrow d^{\mathbf{X}^{\beta}(\tau)})$ are carried out for each target variable β according to Eq. (5) ($\beta = 0, 5$ and 10 are shown in blue, red and green, respectively). The optimal weights from each optimization, depicted in the central bar plots, are used to construct a connectivity matrix G (here, G is built using a single time lag $\tau = 1$). From this matrix, dynamical communities are identified and depicted on a graph, where several variables are grouped within the same node.

maximum weights over the tested values of τ are stored as columns of a $D \times D$ matrix G :

$$G^{\alpha\beta} = \max_{\tau} \hat{w}_{\beta}^{\alpha}. \quad (6)$$

We note that this procedure can be seen as a non-linear generalization of multivariate Granger causality [15, 16]. Constructing d^A over a single time frame provides the correct results when the lag of direct links is not larger than 1 in the underlying time series graph. In the SM we describe how our approach can be extended when this condition does not hold, constructing d^A on multiple time frames.

Ideally, each autonomous set \mathcal{S}^{β} can be directly extracted from the elements $G^{\alpha\beta}$ that are nonzero. However, in applications the G matrix is estimated using a finite number of measures (or a finite trajectory). Therefore, one can decide if an element is zero only according to a specified tolerance: we then set $X^{\alpha} \in \mathcal{S}^{\beta}$ whenever $G^{\alpha\beta} > \varepsilon$. The threshold ε is the main hyper parameter of our algorithm. A false negative may appear if the coupling that we aim to detect by testing $\hat{w}_{\beta}^{\alpha} > 0$ is present but weak. This may occur, for example, when X^{α} causes X^{β} indirectly via several mediating variables.

To account for false negatives, we first construct a directed graph represented by the set of links for which $G^{\alpha\beta} > \varepsilon$, and then we construct each autonomous set \mathcal{S}^{β} as the full set of ancestors of X^{β} . This can be done efficiently with an algorithm similar in spirit to that of Breadth First Search [21]: one starts with a set of ancestors \mathcal{A} containing only the node itself. Then one updates \mathcal{A} including all the nodes with links directed to \mathcal{A} . This procedure is repeated recursively until no more nodes are added to \mathcal{A} . Using this procedure, missing links $X^{\alpha} \rightarrow X^{\beta}$ are likely to be recovered through indirect paths $X^{\alpha} \rightarrow X^{\gamma} \rightarrow \dots \rightarrow X^{\beta}$.

ii) Identification of dynamical communities — We then use the sets \mathcal{S}^{β} to build a hierarchy between groups of variables, assigning to each group a specific level of autonomy. The “most autonomous” groups evolve independently, while the “least autonomous” are influenced at different extent by the evolution of other groups. We refer to such groups as *dynamical communities*. The concept of dynamical communities is rooted in the preliminary notion of *minimal autonomous sets*, which we define as the smallest disjoint sets among all \mathcal{S}^{β} . By construction, any variable of a minimal autonomous set is a direct or indirect cause of any other variable in the same set.

We say that \mathcal{G}_k is a dynamical community with level of autonomy $l(\mathcal{G}_k)$ ($l(\mathcal{G}_k) = 0, 1, 2, \dots$) if \mathcal{G}_k is minimally autonomous when all the variables in dynamical communities of lower levels are removed. For example, \mathcal{G}_k is a dynamical community with level 3 if all the variables in the sets \mathcal{G}_m with levels $l(\mathcal{G}_m) = 0, 1$ or 2 are not considered. This construction directly reveals a well-defined hierarchy of autonomy: if a group has level of autonomy k , then it can be caused only by groups with level $m < k$, and, in turn, it can cause only groups with level $m > k$, while no links can be present among groups at the same level.

To find all the dynamical communities and their levels of autonomy, we proceed as follows. First, we identify the minimal autonomous sets among all \mathcal{S}^β . Such groups define the dynamical communities of level zero, which are groups evolving independently of all the rest of the system. Then, we subtract from the remaining \mathcal{S}^β all the variables belonging to the dynamical communities already identified, and we repeat the search of the new minimal autonomous sets. The new communities are assigned a level of autonomy equal to 1. If subtracting the variables found at the previous step results in empty sets, such sets are discarded. This procedure is repeated, increasing at each step the level of autonomy, until no sets remain.

iii) Construction of the community causal graph — The causal connections between the dynamical communities are depicted using a directed acyclic graph where each node represents a dynamical community \mathcal{G}_k , which we name *community causal graph* (see Fig. 1). We draw a directed arrow $\mathcal{G}_k \rightarrow \mathcal{G}_m$ if $l(\mathcal{G}_m) = l(\mathcal{G}_k) + 1$ and if there is at least a pair of variables $X^\alpha \in \mathcal{G}_k$ and $X^\beta \in \mathcal{G}_m$ such that $X^\alpha \rightarrow X^\beta$.

Results — We tested our approach on trajectories generated by dynamical systems of different complexity. Specifically, we considered three groups of five coupled logistic maps (Figs. 2a-c), five coupled Lorenz oscillators [22] (Figs. 2d-f), and two 40-dimensional Lorenz 96 systems [23] unidirectionally coupled (Figs. 2g-i). Since deterministic relationships are known to violate a condition known as faithfulness [2, 9], which is necessary to infer the correct causal structure from conditional independencies, we added a small white noise to each variable while integrating the dynamic equations (see SM). For each system, distances entering the DII optimization at step i) of the algorithm were computed by extracting $N = 2000$ frames, used as independent initial conditions, from a single time series realization.

The left panels in Fig. 2 show the community graphs produced by the algorithm when the threshold ε is set to the average value of the weights in matrix G (black star marker in the right panels). These graphs reproduce the correct connectivity read from the ground-truth equations: all variables grouped in a single node are dynamically intertwined, namely each one is a direct or indirect cause of any other variable, and an arrow between two groups at consecutive levels is present when at least two

variables, one per group, are interacting. The central panels show the all-variable graphs built from the matrix $G^{\alpha\beta} > \varepsilon$, with nodes colored according to the level of autonomy assigned to the corresponding groups at step ii). This matrix was computed according to Eq. (6), with $\tau_{\max} = 1$ for the top row example, $\tau_{\max} = 60$ for the middle row, and $\tau_{\max} = 30$ for the top row example.

The outcome of the algorithm is influenced by the choice of the threshold ε . In Fig. 2, right column, we validated the correctness of the recovered dynamical communities and their connectivity separately, by measuring as a function of ε the adjusted mutual information [24] between the true groups and the recollected ones (right panels, blue solid curves), and the accuracy of the all-variable adjacency matrix obtained from the final community graphs (right panels, dashed red curves). Both measures are defined in the range $[0, 1]$, with 1 being the case of optimal reconstruction. We refer to the SM for a formal definition of these measures. Remarkably, in all systems we observe a wide range of threshold values leading to an exact reconstruction. In all three examples, the rule-of-thumb criterion of choosing ε as the average of all weights provides a value of the threshold within the correct interval.

Discussion — We have demonstrated that our approach can efficiently reconstruct the causal structure underlying high-dimensional dynamical systems, providing a coarse-grained visualization of the system’s causal connectivity. The most relevant feature of our method is that the number of optimizations — analogous to conditional independence tests — scales linearly with the number of variables, and still the approach is able to capture “multi-body” synergistic causal effects that are hard to detect by constructing conditioning sets of increasing size [2].

Outside the field of causal discovery, alternative methods have been developed to identify clusters of dynamical variables with strong intra-cluster and weak inter-cluster interactions [25–28]. However, such methods also rely on combinatorial searches of subsets, and typically require greedy or metaheuristic implementations to be practically applied to high-dimensional systems [26, 29].

The outcome of our algorithm depends on the choice of the threshold parameter ε , for which we heuristically found that the average of the weights in matrix G appears as a viable choice. Our approach may be improved by estimating the statistical confidence on each element of G and fixing a threshold on this confidence.

Our approach could be useful for analyzing high-dimensional systems such as a brain connectivity network, where time series graphs become unmanageable [9]. In these scenarios an all-variable representation of the dynamics may hinder its basic features, by producing a graph which, even if correct, is in practice very difficult to read. Moreover, real-world time series often result from processes that are continuous in time. In such cases, the inferrable time lag is limited by the achievable sampling time [2]. This may introduce artifacts for processes in which the interactions are approximately in-

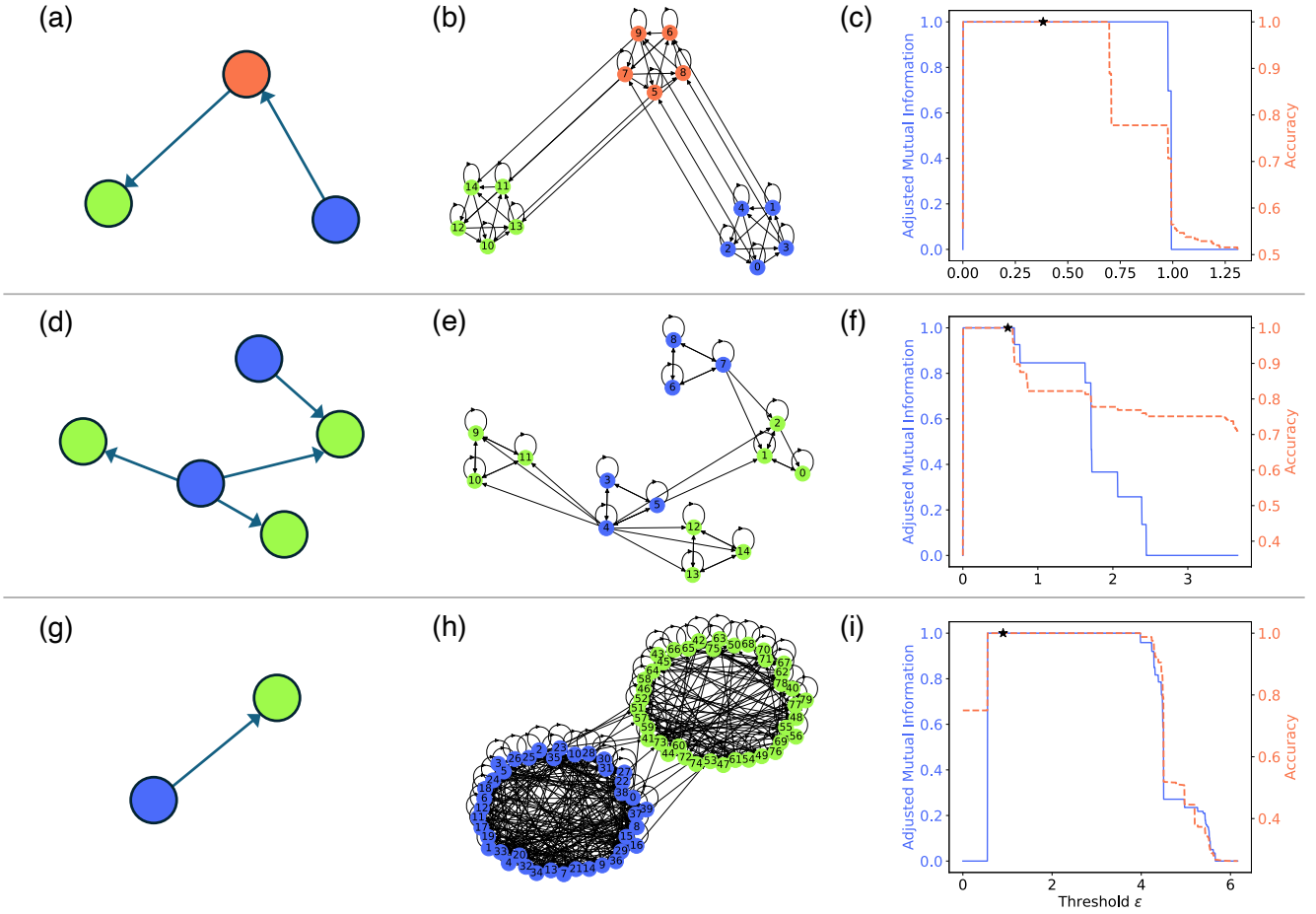


FIG. 2. Outcome and performance of the algorithm in three different test cases: (a)-(c) 15 coupled logistic maps, (d)-(f) 5 coupled Lorenz systems and (g)-(i) 2 Lorenz 96 systems. Left panels (a),(d) and (g): community causal graphs produced by the algorithm, which correctly retrieves the ground-truth connectivity. Central panels (b), (e) and (h): all-variable graphs obtained from condition $G^{\alpha\beta} > \varepsilon$, setting ε to 0.38, 0.6 and 3.5, respectively. Nodes in community and all-variable graphs are colored according to the autonomous levels identified in step ii). Right panels (c), (f) and (i): validation measures of the recovered connectivity as a function of the threshold parameter ε , in the range $[0, \max_{\alpha\beta (\alpha \neq \beta)} G^{\alpha\beta}]$. For larger values of ε , no pairs of variables are found to be linked. Blue solid curve: adjusted mutual information between the retrieved groups and the ground-truth ones. Red dashed curve: accuracy of the all-variable adjacency matrix recovered from the final community graph, defined as the fraction of correctly identified links. Black star marker: results by setting the threshold ε to the average of all weights in $G^{\alpha\beta}$.

stantaneous compared to the observation time scale, as those described by classical ordinary differential equations (ODEs). For these reasons, while methods for inferring the time series causal graph may be a valid option for low-dimensional systems whose dynamics is well representable by discrete-time structural causal models [1], our framework presents an efficient and promising alternative in high-dimensional time series generated by continuous processes. In these system it is useful choosing the time lag τ according to Eq. (6). This allows getting rid of a hyperparameter which, in other approaches, is simply held fixed to the time difference between two successive observations of the system. In the SM (Fig. S2) we show that using $\tau = 1$ would significantly decrease the detection power of the algorithm.

The codes implementing our algorithm and their documentation are available in the Python library DADaPy [30].

SUPPLEMENTAL MATERIAL

I. RELATION WITH CONDITIONAL INDEPENDENCIES AND CONSTRAINT-BASED METHODS

In this section we draw a connection between our framework and the language of conditional independencies employed in constraint-based methods for causal discovery, which we briefly review in the following. We refer to refs. [1, 2] for a more comprehensive overview of this framework.

A. Structural causal models and time series graphs

As a starting point, one assumes the existence of an (unknown) “structural causal model” (SCM) generating the data, which consists of a set of time-discrete equations ($t \in \mathbb{Z}$) of the form

$$X^\alpha(t) := f^\alpha(pa(X^\alpha(t)), \eta^\alpha(t)) \quad (\alpha = 1, \dots, D). \quad (\text{S1})$$

In Eq. (S1), $\{X^\alpha(t)\}$ are the observed (or endogenous) variables, $\{f^\alpha\}$ are functions called causal mechanisms, $pa(X^\alpha(t))$ is a set containing the variables $X^\beta(t - \tau)$ ($\tau \in \mathbb{N}$) that directly cause $X^\alpha(t)$, also called parents of $X^\alpha(t)$, and $\{\eta^\alpha(t)\}$ are external (or exogenous) variables, typically modeled as noise terms [6, 31]. Here, we focus on the case in which the cause precedes its effect, although the case of contemporaneous links can also be addressed [13]. The time series graph representing the relations in Eq. (S1) can be constructed by drawing a link $X^\beta(t - \tau) \rightarrow X^\alpha(t)$ whenever $X^\beta(t - \tau) \in pa(X^\alpha(t))$. This gives rise to an infinite directed acyclic graph (DAG).

If the noise terms are assumed to be independent of each other, one can exclude the presence of unobserved common drivers, namely external variables that are causes of two or more endogenous variables. Given this condition, known as causal sufficiency, and the fact that the underlying graph is by construction a DAG, the joint distribution of the endogenous variables can be written in a factorized form:

$$p(\{X^\alpha(t)\}) = \prod_{\alpha, t} p(X^\alpha(t) | pa(X^\alpha(t))). \quad (\text{S2})$$

The causal structure of the model can be equivalently written in terms of conditional independencies, through the so-called causal Markov condition:

$$X^\alpha(t) \perp\!\!\!\perp X^\beta(t + \tau) | pa(X^\beta(t + \tau)) \quad (\forall \alpha, \beta = 1, \dots, D; \forall t \in \mathbb{Z}; \forall \tau > 0). \quad (\text{S3})$$

In words, the causal Markov condition ensures that, conditional on the set of all its direct causes [32], each variable is independent of all variables which are not its effects.

In the particular case in which the SCM does not vary over time, the time series graph is an infinite repetition of the same causal patterns and we can ease the notation as:

$$X^\alpha(0) \perp\!\!\!\perp X^\beta(\tau) | pa(X^\beta(\tau)) \quad (\forall \alpha, \beta = 1, \dots, D; \forall \tau > 0). \quad (\text{S4})$$

Using the graphical criterion of d-separation [5, 9], conditional independencies of the form given in Eq. (S4) can be directly inferred from the structure of the time series graph. All the methods discussed in the following paragraphs are also based on the assumption that every measurable conditional independence corresponds to d-separation among the variables in the graph. This assumption is known as faithfulness [2, 6]. The Markov condition and the faithfulness assumption ensure that the structure of Eqs. (S1) can be fully characterized in terms of conditional independencies [7, 8]. Such independencies are commonly inferred from data using conditional mutual information or partial correlation.

Under the assumptions specified above, causal discovery methods that aim to infer the specific lags of the interactions for each pair of nodes $X^\alpha(t)$ and $X^\beta(t + \tau)$ will be here referred to as “lag-specific”. In contrast, we call “lag-unspecific” those methods that only aim to understand if a link between $X^\alpha(t)$ and $X^\beta(t + \tau)$ is present for any τ .

B. Lag-specific methods - Full conditioning

We now discuss two strategies that can be adopted to find the parents of each node in the causal graph.

The first strategy consists in performing independence tests among a variable $X^\beta(\tau)$ and a variable $X^\alpha(0)$, while conditioning on the full history of the trajectory up to time τ , denoted as $\mathbf{X}(\tau^-) := (\mathbf{X}(\tau-1), \mathbf{X}(\tau-2), \dots)$, excluding $X^\alpha(0)$. It can be easily shown that independence is found only if $X^\alpha(0)$ is not among the parents of $X^\beta(\tau)$. This strategy, called ‘‘Full Conditional Independence’’ (FullCI) by Runge *et al.* [2, 12], corresponds to case (a) in Table S1 and Fig. S1. In practical implementations, the past of $X^\beta(\tau)$ is included up to a maximum time lag τ_{\max} , which is supposed to be larger than the maximum lag among all direct links [1]. This method is algorithmically efficient, as it requires a single conditional independence test between each pair of variables, but is affected by a high rate of false negative detections [12]. The reason for this drawback is that, when $X^\alpha(0) \in pa(X^\beta(\tau))$, $\mathbf{X}(\tau^-)$ is likely to contain many variables that, although not necessary to assess whether $X^\alpha(0) \rightarrow X^\beta(\tau)$, explain part of the dependence between $X^\alpha(0)$ and $X^\beta(\tau)$.

C. Lag-specific methods - Optimal conditioning

Another possible strategy is to search, among all subsets of $\mathbf{X}(\tau^-)$, for a subset S for which $X^\alpha(0) \perp\!\!\!\perp X^\beta(\tau) \mid S \setminus X^\alpha(0)$. If no such subset exists, then $X^\alpha(0)$ must be a parent of $X^\beta(\tau)$. When this occurs, the search for S does not stop until all conditioning sets have been tested. If all possible sets are considered, this results in a combinatorial explosion in the number of tests to be performed. In practical applications, $\mathbf{X}(\tau^-)$ is constructed by including all variables up to a maximum time lag in the past. This second class of approaches includes standard algorithms such as PC [6, 11] or IC [5, 10], designed for time-independent causal graphs, and modern approaches developed for time series data, such as PCMCI [12] and PCMCI+ [13], which employ strategies to reduce the dimension of the search space. We consider PCMCI as representative of this class of methods (see case (b) in Table S1 and Fig. S1). PCMCI can detect the presence of conditional dependencies building at each step conditioning sets of minimal size, without introducing variables that may increase the false negative rate of conditional dependence measures.

D. Lag-unspecific methods - Multivariate Granger Causality / Transfer Entropy

Multivariate Granger Causality (GC) [14–16] and Transfer Entropy (TE) [17] can be seen as lag-unspecific versions of the FullCI approach, where $X^\alpha(0)$ is replaced by the full history of X^α up to $t = \tau - 1$, denoted by $\mathbf{X}^\alpha(\tau^-)$ (see case (c) in Table S1 and Fig. S1). Also in this case, $\mathbf{X}^\alpha(\tau^-)$ is constructed with frames up to a maximum time lag τ_{\max} in the past. In the case of multivariate GC, the conditional independence test is practically implemented by fitting separately two vector autoregressive models for $X^\beta(\tau)$, one including the whole past $\mathbf{X}(\tau^-)$, and one including only $\mathbf{X}(\tau^-) \setminus \mathbf{X}^\alpha(\tau^-)$. Here, lag-unspecific means that condition $\mathbf{X}^\alpha(\tau^-) \perp\!\!\!\perp X^\beta(\tau) \mid \mathbf{X}(\tau^-) \setminus \mathbf{X}^\alpha(\tau^-)$ allows inferring the existence of at least a direct link $X^\alpha(0) \rightarrow X^\beta(\tau)$, but not the specific value of τ . The advantages and drawback of this framework are similar to those of FullCI.

E. Connection between DII approach and conditional independencies

By employing the DII as a metric for conditional independence, we can convert causal discovery into an optimization problem.

In ref. [20] we employed Eq. (2) of the main text,

$$\hat{w} = \underset{w}{\operatorname{argmin}} \Delta(d^{wX(0), Y(0)} \rightarrow d^{Y(\tau)}) \neq 0 \quad (\text{S5})$$

as a condition to assess whether $X(0) \perp\!\!\!\perp Y(\tau) \mid Y(0)$. Similarly, in the generalization considered in this work,

$$\hat{w}_\beta = \underset{w}{\operatorname{argmin}} \Delta\left(d^{w \odot \mathbf{X}(0)} \rightarrow d^{X^\beta(\tau)}\right), \quad (\text{S6})$$

we considered $\hat{w}_\beta^\alpha \neq 0$ - where \hat{w}_β^α denotes the α -component of \hat{w}_β - to assess the conditional independence relationship $X^\alpha(0) \perp\!\!\!\perp X^\beta(\tau) \mid \mathbf{X}(0) \setminus X^\alpha(0)$. As in GC-inspired approaches, this method enables the identification of multi-body interactions, characterized by multiple components of w being nonzero simultaneously. In supplementary section III we show how our approach can be extended to include consecutive time frames in the optimized distance space, resulting in a practical implementation of the conditioning test $\mathbf{X}^\alpha(0^-) \perp\!\!\!\perp X^\beta(\tau) \mid \mathbf{X}(0^-) \setminus \mathbf{X}^\alpha(0^-)$.

Even with this extension, a key distinction remains between our conditioning strategy (case (d) in Table S1 and Fig. S1) and that employed in multivariate GC / TE. Specifically, we allow for time lags $\tau \neq 1$ between the conditioning

set in the past and the target variable in the future, without including the intermediate frames in the conditioning. We observed that this is particularly relevant when analyzing time series generated by time-continuous processes. Indeed, in these cases the conditional dependence between $X^\alpha(0)$ and $X^\beta(\tau)$ can be more easily detected by our approach for $\tau > 1$, even though the ground-truth interaction occurs at shorter time scales. As shown in Fig. S2, using $\tau = 1$, which is equivalent to condition up to the immediate past of the target variable, can significantly degrade the reconstruction power of our algorithm. The parameter τ has no direct counterpart in standard approaches for causal graph reconstruction, aside from the conditional mutual information introduced by Paluš *et al.* [33], Paluš and Vejmelka [34].

We highlight that the use of $\tau \neq 1$ is only possible in a lag-unspecific framework as that considered here, where no distinction between direct and indirect causes is made.

	Conditioning test	Type
(a) FullCI [2]	$X^\alpha(0) \perp\!\!\!\perp X^\beta(\tau) \mid \mathbf{X}(\tau^-) \setminus X^\alpha(0)$	lag-specific
(b) PCMCI [12]	$X^\alpha(0) \perp\!\!\!\perp X^\beta(\tau) \mid \hat{p}a(X^\alpha(0)) \cup \hat{p}a(X^\beta(\tau))$	lag-specific
(c) Multivariate GC [14–16] / TE [17]	$\mathbf{X}^\alpha(\tau^-) \perp\!\!\!\perp X^\beta(\tau) \mid \mathbf{X}(\tau^-) \setminus \mathbf{X}^\alpha(\tau^-)$	lag-unspecific
(d) Our approach	$X^\alpha(0) \perp\!\!\!\perp X^\beta(\tau) \mid \mathbf{X}(0) \setminus X^\alpha(0)$	lag-unspecific

TABLE S1. Comparison of different conditioning strategies for time series causal discovery. The independence relationship shown in “conditioning test” corresponds to the null hypothesis of X^α being non-causal to X^β , either in a (a)-(b) lag-specific or (c)-(d) lag-unspecific fashion. In case (b), $\hat{p}a(X^\alpha(0))$ and $\hat{p}a(X^\beta(\tau))$ denote the inferred set of parents of $X^\alpha(0)$ and $X^\beta(\tau)$, as the ground-truth sets are unknown.

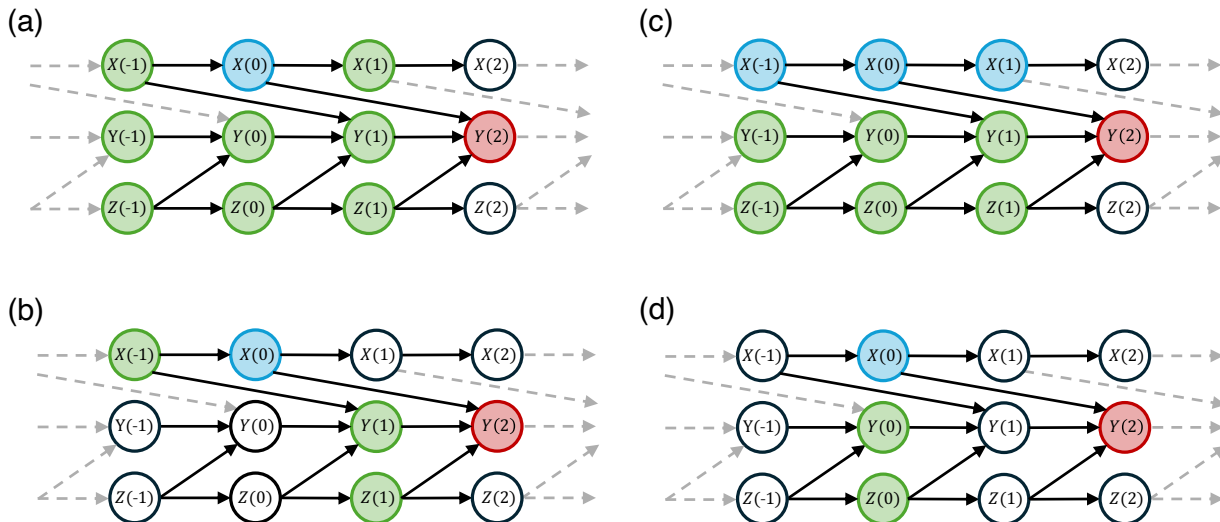


FIG. S1. Visualization of different conditioning approaches on a time series graph: (a) FullCI [2], (b) PCMCI [12], (c) multivariate Granger Causality [14–16] / Transfer Entropy [17], and (d) our approach. (a) and (b) are lag-specific strategies, while (c) and (d) are lag-unspecific.

II. DETAILS ON TEST SYSTEMS

In this section we provide details on the test systems employed in the validation tests. To write the equations in a compact form, we use indices μ, ν to identify different dynamical communities and indices α, β to represent variables within the same community. Trajectories of 10^5 time frames were generated for all systems. The first 10^4 samples of each trajectory were then discarded to eliminate equilibration artifacts.

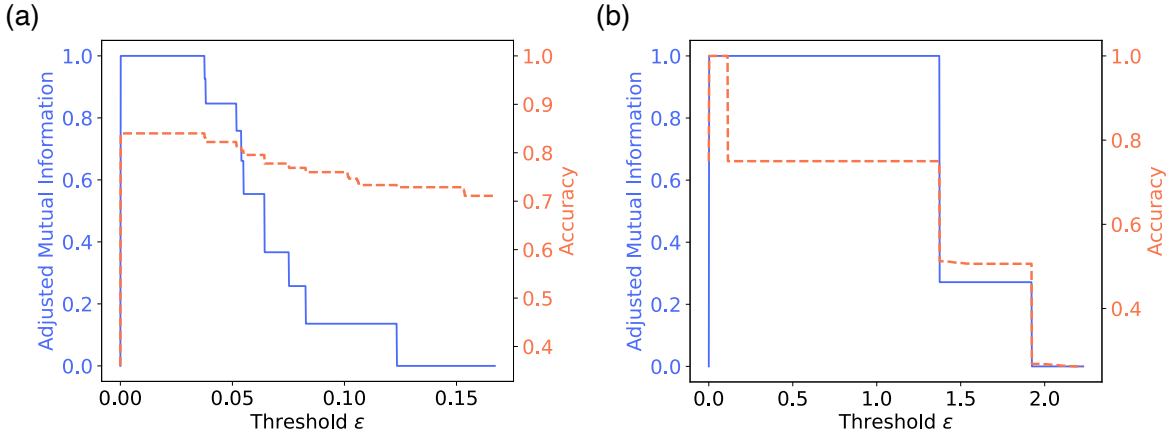


FIG. S2. Validation measures referred to (a) the five coupled Lorenz systems and (b) the two coupled Lorenz 96 systems, computing the connectivity matrix G with $\tau_{\max} = 1$. In case (a), no choice of the threshold parameter ε allows for a correct reconstruction of the community graph.

A. Logistic maps

The equations of the noisy coupled logistic maps shown in Figs. 1 and 2a of the main text, structured in three communities with five variables each ($\mu, \nu \in \{0, 1, 2\}$; $\alpha, \beta \in \{0, 1, 2, 3, 4\}$), read:

$$X_{\mu}^{\alpha}(t+1) = X_{\mu}^{\alpha}(t) \cdot \left(r_{\mu}^{\alpha} - r_{\mu}^{\alpha} \cdot X_{\mu}^{\alpha}(t) - \sum_{\beta=0}^4 c_{\mu}^{\beta\alpha} X_{\mu}^{\beta}(t) - \sum_{\nu=0}^2 d_{\nu\mu}^{\alpha} X_{\nu}^{\alpha}(t) + \sigma \mathcal{R}_{\mu}^{\alpha}(t) \right) \text{ mod } 1. \quad (\text{S7})$$

The terms $\sigma \mathcal{R}_{\mu}^{\alpha}(t)$, where $\sigma = 0.1$ and $\mathcal{R}_{\mu}^{\alpha} \sim \mathcal{N}(0, 1)$, are independent white noises added to all variables of the system. The coefficients $c_{\mu}^{\beta\alpha}$ tune the strength of the interactions within the same community, while the couplings $d_{\nu\mu}^{\alpha}$ control the interactions between different communities. For each α , we chose the parameters r_{μ}^{α} by sampling uniformly 10 values in $(3.68, 4)$, and setting $r_0^{\alpha} = r_1^{\alpha} \neq r_2^{\alpha}$. Within each community μ we considered $c_{\mu}^{\beta\alpha} = \delta_{\beta, \alpha-1} + 0.5 \delta_{\beta, \alpha+2}$, with conventions $x_{\mu}^{-1} = x_{\mu}^4$ and $x_{\mu}^5 = x_{\mu}^0$, and for each variable α in community μ we set the interaction with variables of other communities as $d_{\nu\mu}^{\alpha} = 0.5 (\delta_{\nu, 1} \delta_{\mu, 2} + \delta_{\nu, 2} \delta_{\mu, 3})$. The connectivity of the system is depicted in Fig. 1 of the main text.

B. Lorenz systems

The system of 5 coupled Lorenz systems ($\mu, \nu \in \{0, 1, 2, 3, 4\}$) is described by the following differential equations, reported here for a single system (or community) μ :

$$\begin{cases} \dot{X}_{\mu}^0 = 10(X_{\mu}^1 - X_{\mu}^0) \\ \dot{X}_{\mu}^1 = X_{\mu}^0(28 - X_{\mu}^2) - X_{\mu}^1 + c \sum_{\nu=0}^4 d_{\nu\mu} (X_{\nu}^0)^2 \\ \dot{X}_{\mu}^2 = X_{\mu}^0 X_{\mu}^1 - \frac{8}{3} X_{\mu}^2 \end{cases} . \quad (\text{S8})$$

The coupling strength was fixed to $c = 0.3$ and $d_{\nu\mu}$, which defines the interaction topology among communities (Fig. 2e of the main text), was set to

$$d = \begin{pmatrix} 0 & 0 & 0 & 0 & 0 \\ 1 & 0 & 0 & 1 & 1 \\ 1 & 0 & 0 & 0 & 0 \\ 0 & 0 & 0 & 0 & 0 \\ 0 & 0 & 0 & 0 & 0 \end{pmatrix} . \quad (\text{S9})$$

Eqs. (S8) were integrated using the `integrate.solve_ivp` function from the SciPy Python library [35]. The trajectory was calculated with a sampling time of $\delta t = 0.003$. A zero-mean Gaussian noise with standard deviation $\sigma = 0.1$ was added independently to each variable in the integration procedure to introduce a stochastic effect.

C. Lorenz 96 systems

The two unidirectionally coupled Lorenz 96 systems of 40 variables each ($\mu, \nu \in \{0, 1\}$, $\alpha, \beta \in \{0, 1, \dots, 39\}$) are defined by the following ordinary differential equations:

$$\dot{X}_\mu^\alpha = (X_\mu^{\alpha+1} - X_\mu^{\alpha-2})X_\mu^{\alpha-1} - X_\mu^\alpha + F_\mu + c\delta_{\mu,1}X_0^\alpha, \quad (\text{S10})$$

where $X_\mu^{-1} = X_\mu^{39}$, $X_\mu^{40} = X_\mu^0$, $F_0 = 5$, $F_1 = 6$, and $c = 0.75$. Eqs. (S10) were integrated with time step $dt = 0.03$ using the LSODA integrator implemented in the SciPy function `integrate.ode_int` [35], saving the trajectory with sampling stride equal to 2. After each integration step, a random Gaussian number with zero mean and variance $\sigma^2 = (0.1)^2$ was independently added to each variable.

In the Lorenz and Lorenz 96 systems, the coupling terms among communities have the same functional form employed in ref. [20].

III. GENERALIZATION TO TIME WINDOWS

In the main text, we presented our approach constructing distance d^A with all variables at a single time frame ($t = 0$), assuming that the maximum lag of direct links is not larger than 1 in the underlying time series graph. Here we show how the conditioning should be extended to multiple frames when this assumption does not hold, and how this can be simply achieved by constructing d^A on a time window rather than on a single time frame.

We use as illustrative example the following three coupled logistic maps:

$$\begin{cases} X(t+1) = X(t) \cdot (r_X - r_X \cdot X(t) + \sigma \mathcal{R}_X(t)) \bmod 1 \\ Y(t+1) = Y(t) \cdot (r_Y - r_Y \cdot Y(t) - c \cdot X(t-1) + \sigma \mathcal{R}_Y(t)) \bmod 1 \\ Z(t+1) = Z(t) \cdot (r_Z - r_Z \cdot Z(t) - c \cdot X(t) + \sigma \mathcal{R}_Z(t)) \bmod 1 \end{cases} \quad (\text{S11})$$

The terms $\sigma \mathcal{R}_\alpha(t)$ ($\alpha = X, Y, Z$), where $\sigma = 0.1$ and $\mathcal{R}_\mu^\alpha \sim \mathcal{N}(0, 1)$ are three independent white noises. The parameters r_X , r_Y , and r_Z were randomly sampled in the interval $(3.68, 4)$, resulting in $r_X \simeq 3.863$, $r_Y \simeq 3.861$ and $r_Z \simeq 3.836$. As for the other systems, a time series of 10^5 samples was generated, discarding the first 10^4 initial points and then sampling $N = 2000$ independent initial conditions for the DII optimization.

According to Eqs. (S11), X causes Y with lag 2 and X causes Z with lag 1. The time series graph of the process is shown in Fig. S3. In this example, the dynamical communities are simply $\{X\}$, $\{Y\}$ and $\{Z\}$, and the community graph is $\{Z\} \leftarrow \{X\} \rightarrow \{Y\}$. Hereafter we will focus on $Y(\tau = 1)$ as target variable of the DII optimization (red node in the time series graphs of Fig. S3).

Fig. S3a shows the application of our approach according to Eq. (5) in the main text, namely minimizing DII ($d^{\mathbf{w} \odot \mathbf{X}(0)} \rightarrow d^{Y(\tau=1)}$) with $\mathbf{X}(0) = (X(0), Y(0), Z(0))$. In this case, a spurious weight associated to $Z(0)$ appears due to the presence of an open path $Z(0) \leftarrow X(-1) \rightarrow Y(1)$. The term ‘‘open’’ and ‘‘closed’’ (or ‘‘blocked’’) are used here in the sense of d-separation [2, 9]: two variables in the graph are conditionally dependent when they are connected by at least an open path. The non-zero weight associated to $Z(0)$ affects the reconstruction quality of the algorithm, resulting in a limited range of the threshold ε providing the correct community graph.

To overcome this problem, we can construct the first distance space as $d^{\mathbf{w} \odot \mathbf{X}_E(0^-)}$, where $\mathbf{X}_E(0^-)$ is the time window of E frames including all variables from $t = -E + 1$ to $t = 0$, namely

$$\mathbf{X}_E(0^-) = \left(\underbrace{X(0), Y(0), Z(0)}_{\mathbf{X}(0)}, \underbrace{X(-1), Y(-1), Z(-1)}_{\mathbf{X}(-1)}, \dots, \underbrace{X(-E+1), Y(-E+1), Z(-E+1)}_{\mathbf{X}(-E+1)} \right). \quad (\text{S12})$$

In turn, \mathbf{w} denotes in this case a vector of $3E$ components (or, more in general, $D \cdot E$ components, where D is the number of variables). Setting $E = 2$ (Fig. S3b) allows including $X(-1)$ in the conditioning set, blocking the path $Z(0) \leftarrow X(-1) \rightarrow Y(1)$. In this case, no spurious weight associated to Z appears, and the community graph reconstruction is correct for almost all values of ε in the interval $[0, \max_{\alpha \neq \beta} G^{\alpha\beta}]$. The same occurs using a larger window ($E = 3$, Fig. S3c).

In general, as can be easily demonstrated, constructing d^A on E consecutive frames enables the application of our conditioning approach without errors, assuming that the maximum lag of direct links in the underlying time series graph is E .

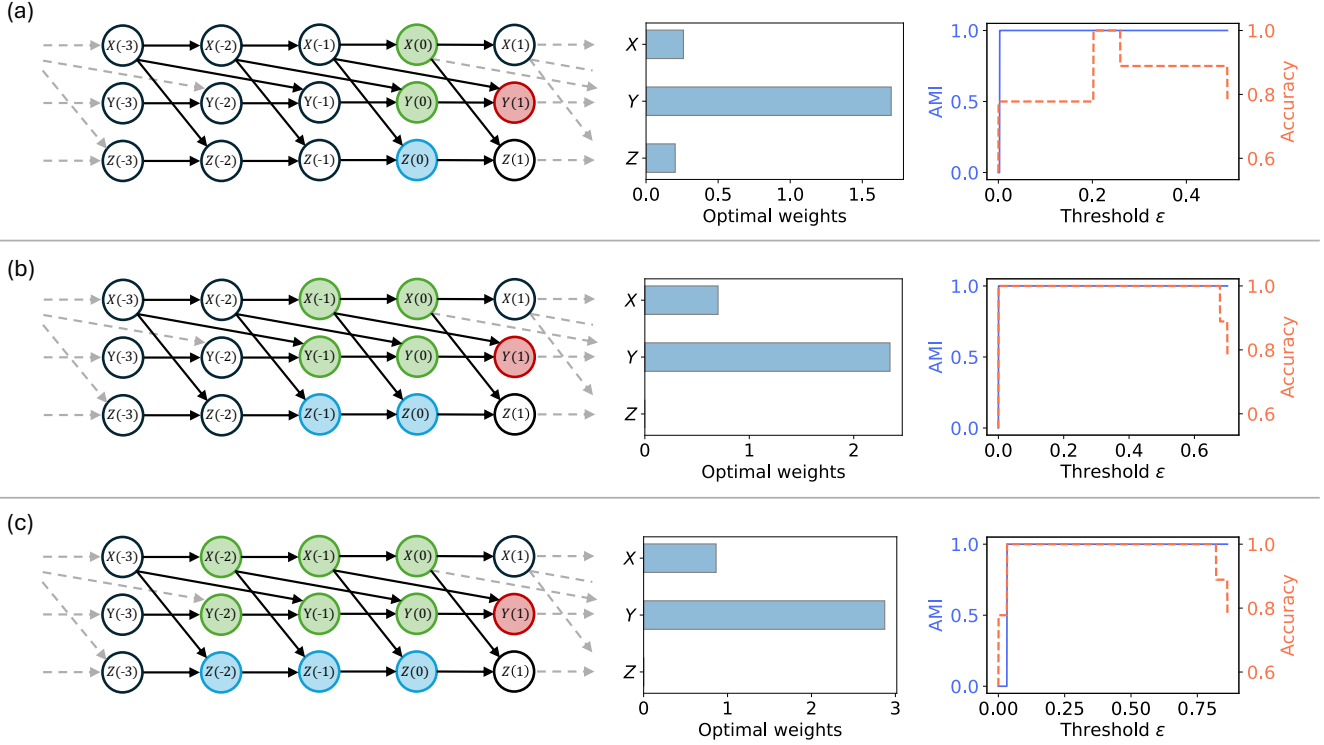


FIG. S3. Extension of the method to time windows, using three noisy coupled logistic maps. The time series graphs in (a), (b) and (c) show the construction of the distance d^A over different number of frames ($E = 1, 2$ and 3 , respectively), including all variables represented by green and blue nodes. The central bar plots show the optimal DII weights using as target variable $Y(1)$ (red node in the time series graphs). When $E > 1$, only the largest weight across different frames is shown for each variable. On the right, the adjusted mutual information (AMI) and the accuracy of the retrieved connectivity matrix are plotted as a function of the threshold parameter ε , in the range $[0, \max_{\alpha, \beta (\alpha \neq \beta)} G^{\alpha, \beta}]$.

IV. DETAILS ON THE DII OPTIMIZATION

In this section, we provide details on the DII optimization process. The code, available in the Python package DADApY [30], was implemented in JAX [36].

A. Neighborhood size parameter λ

An important parameter appearing in Eq. (4) of the main text is λ , which defines the size of the neighbourhoods in the first distance space. The classical Information Imbalance is recovered in the limit $\lambda \rightarrow 0$; however, excessively small λ values can hinder the optimization process, as the DII derivatives approach zero in this regime [19]. To address this issue, we employed a point-adaptive scheme for computing λ , assigning a distinct value λ_i to each point i in the sum of Eq. (4) in the main text. In this formulation, the standard Information Imbalance is recovered in the limit $\lambda_i \rightarrow 0, \forall i = 1, \dots, N$. The use of a point-specific λ_i is particularly beneficial when the data set features a non-homogeneous point distribution. In this case, relying on a single distance scale could result in inconsistent neighborhood sizes across different regions of the data manifold. Each λ_i was computed as

$$\lambda_i = 0.1 d_{i, j^{(k)}}^A(\mathbf{w}), \quad (\text{S13})$$

where 0.1 is an empirical prefactor and $j^{(k)}$ is the k -th nearest neighbour of i according to the (squared) distance $d^A(\mathbf{w})$. In this study, k was fixed to 5% of the total number of points used in the DII calculation (namely, $k/N = 0.05$). To account for changes in $d^A(\mathbf{w})$ during the optimization, the parameters λ_i were recomputed after each weight update.

B. Optimization strategy

The convergence of the DII optimization to its global minimum depends on several factors, including the choice of the optimizer and the use of mini-batches. Mini-batching, which involves computing gradients on random subsets of points during each gradient descent update, is a common strategy to improve both convergence speed and stability, particularly when the loss function contains multiple local minima.

In this work, we sampled $N = 2000$ evenly spaced frames from each time series. In the DII optimization, for each training epoch, we randomly partitioned the resulting data set into 20 mini-batches, each containing $N' = 100$ points. Within each mini-batch, the parameter k for determining λ_i was set to 5. The DII optimization was carried out using the Adam optimizer [37], which is well known for its robust convergence properties.

C. Training Schedule

In this work, all DII optimization were carried with 500 training epochs. In each optimization, the learning rate used by the Adam optimizer was set to the initial value of 5×10^{-3} , and gradually decreased to zero according to a cosine decay schedule.

V. VALIDATION MEASURES

The adjusted mutual information (AMI) [24] shown in the right panels of Fig. 2 in the main text is a measure of discrepancy between the dynamical communities retrieved by our algorithm, $\{\mathcal{G}_i\}$, and the ground-truth groups $\{\mathcal{G}_i^{gt}\}$. The sets $U := \{\mathcal{G}_i\}$ and $V := \{\mathcal{G}_i^{gt}\}$ define two possible partitions of the D dynamical variables. We computed the AMI by using the `metrics.adjusted_mutual_info_score` function in SciPy [35], which computes it as:

$$\text{AMI}(U, V) = \frac{I(U, V) - \mathbb{E}[I(U, V)]}{(H(U) + H(V))/2 - \mathbb{E}[I(U, V)]}, \quad (\text{S14})$$

where $I(U, V)$ is the mutual information between the two partitions, $H(U)$ ($H(V)$) is the Shannon entropy associated to partition U (respectively V), and $\mathbb{E}[I(U, V)]$ is the expected mutual information between two random partitions.

To measure the agreement of the retrieved links among dynamical communities with the ground-truth connectivity, we first constructed from the final community graph an all-variable adjacency matrix embedding all direct and indirect links retrieved by the algorithm. Then, we computed the accuracy of this connectivity matrix as the fraction of correctly retrieved links over the total number of links:

$$\text{Accuracy} = \frac{\text{TP} + \text{TN}}{\text{P} + \text{N}}, \quad (\text{S15})$$

where TP (TN) is the number of true positive (negative) link detections, and P (N) is the total number of positive (negative) detections.

-
- [1] J. Runge, A. Gerhardus, G. Varando, V. Eyring, and G. Camps-Valls, Causal inference for time series, *Nature Reviews Earth & Environment* **4** (2023).
 - [2] J. Runge, Causal network reconstruction from time series: From theoretical assumptions to practical estimation, *Chaos: An Interdisciplinary Journal of Nonlinear Science* **28**, 075310 (2018).
 - [3] C. K. Assaad, E. Devijver, and E. Gaussier, Survey and evaluation of causal discovery methods for time series, *J. Artif. Int. Res.* **73**, 10.1613/jair.1.13428 (2022).
 - [4] S. L. Brunton, J. L. Proctor, and J. N. Kutz, Discovering governing equations from data by sparse identification of nonlinear dynamical systems, *Proceedings of the National Academy of Sciences* **113**, 3932 (2016).
 - [5] J. Pearl, *Causality: Models, Reasoning and Inference*, 2nd ed. (Cambridge University Press, USA, 2009).
 - [6] P. Spirtes, C. Glymour, and R. Scheines, *Causation, Prediction, and Search* (The MIT Press, 2001).
 - [7] D. Geiger, T. Verma, and J. Pearl, Identifying independence in bayesian networks, *Networks* **20**, 507 (1990).
 - [8] T. Verma and J. Pearl, Causal networks: Semantics and expressiveness, in *Machine Intelligence and Pattern Recognition*, Machine Intelligence and Pattern Recognition No. C (1990) pp. 69–76, c ed.
 - [9] D. Chicharro and S. Panzeri, Algorithms of causal inference for the analysis of effective connectivity among brain regions, *Frontiers in Neuroinformatics* **8**, 10.3389/fninf.2014.00064 (2014).

- [10] T. Verma and J. Pearl, Equivalence and synthesis of causal models, in *Proceedings of the Sixth Annual Conference on Uncertainty in Artificial Intelligence*, UAI '90 (Elsevier Science Inc., USA, 1990) p. 255–270.
- [11] P. Spirtes and C. Glymour, An algorithm for fast recovery of sparse causal graphs, *Social Science Computer Review* **9**, 62 (1991).
- [12] J. Runge, P. Nowack, M. Kretschmer, S. Flaxman, and D. Sejdinovic, Detecting and quantifying causal associations in large nonlinear time series datasets, *Science Advances* **5**, eaau4996 (2019).
- [13] J. Runge, Discovering contemporaneous and lagged causal relations in autocorrelated nonlinear time series datasets, in *Proceedings of the 36th Conference on Uncertainty in Artificial Intelligence (UAI)*, Proceedings of Machine Learning Research, Vol. 124, edited by J. Peters and D. Sontag (PMLR, 2020) pp. 1388–1397.
- [14] C. W. J. Granger, Investigating causal relations by econometric models and cross-spectral methods, *Econometrica* **37**, 424–438 (1969).
- [15] A. B. Barrett, L. Barnett, and A. K. Seth, Multivariate granger causality and generalized variance, *Phys. Rev. E* **81**, 041907 (2010).
- [16] K. J. Blinowska, R. Kuś, and M. Kamiński, Granger causality and information flow in multivariate processes, *Phys. Rev. E* **70**, 050902 (2004).
- [17] T. Schreiber, Measuring information transfer, *Phys. Rev. Lett.* **85**, 461 (2000).
- [18] A. Glielmo, C. Zeni, B. Cheng, G. Csányi, and A. Laio, Ranking the information content of distance measures, *PNAS Nexus* **1**, pgac039 (2022), <https://academic.oup.com/pnasnexus/article-pdf/1/2/pgac039/53406126/pgac039.pdf>.
- [19] R. Wild, F. Wodaczek, V. Del Totto, B. Cheng, and A. Laio, Automatic feature selection and weighting in molecular systems using differentiable information imbalance, *Nature Communications* **16**, 270 (2025).
- [20] V. Del Totto, G. Fortunato, D. Bueti, and A. Laio, Robust inference of causality in high-dimensional dynamical processes from the information imbalance of distance ranks, *Proceedings of the National Academy of Sciences* **121**, e2317256121 (2024).
- [21] H. T. Cormen, E. C. Leiserson, R. L. Rivest, and C. Stein, *Introduction to Algorithms* (PHI Learning Private Limited, 2017).
- [22] E. N. Lorenz, Deterministic nonperiodic flow, *Journal of Atmospheric Sciences* **20**, 130 (1963).
- [23] E. N. Lorenz, Predictability – a problem partly solved, in *Predictability of Weather and Climate*, edited by T. Palmer and R. Hagedorn (Cambridge University Press, 2006) p. 40–58.
- [24] N. X. Vinh, J. Epps, and J. Bailey, Information theoretic measures for clusterings comparison: is a correction for chance necessary?, in *Proceedings of the 26th Annual International Conference on Machine Learning*, ICML '09 (Association for Computing Machinery, New York, NY, USA, 2009) p. 1073–1080.
- [25] G. Tononi, A. R. McIntosh, D. Russell, and G. M. Edelman, Functional clustering: Identifying strongly interactive brain regions in neuroimaging data, *NeuroImage* **7**, 133 (1998).
- [26] M. Villani, A. Roli, A. Filisetti, M. Fiorucci, I. Poli, and R. Serra, The search for candidate relevant subsets of variables in complex systems, *Artificial Life* **21**, 412 (2015).
- [27] G. D'Addese, L. Sani, L. La Rocca, R. Serra, and M. Villani, Asymptotic information-theoretic detection of dynamical organization in complex systems, *Entropy* **23**, 10.3390/e23040398 (2021).
- [28] G. D'Addese, M. Casari, R. Serra, and M. Villani, A fast and effective method to identify relevant sets of variables in complex systems, *Mathematics* **9**, 10.3390/math9091022 (2021).
- [29] L. Sani, M. Amoretti, S. Cagnoni, M. Mordonini, and R. Pecori, Ress: A tool for discovering relevant sets in complex systems, *SoftwareX* **14**, 100693 (2021).
- [30] A. Glielmo, I. Macocco, D. Doimo, M. Carli, C. Zeni, R. Wild, M. d'Errico, A. Rodriguez, and A. Laio, Dadapy: Distance-based analysis of data-manifolds in python, *Patterns* **3**, 100589 (2022).
- [31] C. K. Assaad, E. Devijver, and E. Gaussier, Survey and evaluation of causal discovery methods for time series, *J. Artif. Int. Res.* **73**, 10.1613/jair.1.13428 (2022).
- [32] D. M. Hausman and J. Woodward, Independence, invariance and the causal markov condition, *British Journal for the Philosophy of Science* **50**, 521–583 (1999).
- [33] M. Paluš, V. Komárek, Z. c. Hrn číř, and K. Štěrbová, Synchronization as adjustment of information rates: Detection from bivariate time series, *Phys. Rev. E* **63**, 046211 (2001).
- [34] M. Paluš and M. Vejmelka, Directionality of coupling from bivariate time series: How to avoid false causalities and missed connections, *Phys. Rev. E* **75**, 056211 (2007).
- [35] P. Virtanen, R. Gommers, T. E. Oliphant, M. Haberland, T. Reddy, D. Cournapeau, E. Burovski, P. Peterson, W. Weckesser, J. Bright, S. J. van der Walt, M. Brett, J. Wilson, K. J. Millman, N. Mayorov, A. R. J. Nelson, E. Jones, R. Kern, E. Larson, C. J. Carey, Í. Polat, Y. Feng, E. W. Moore, J. VanderPlas, D. Laxalde, J. Perktold, R. Cimrman, I. Henriksen, E. A. Quintero, C. R. Harris, A. M. Archibald, A. H. Ribeiro, F. Pedregosa, P. van Mulbregt, and SciPy 1.0 Contributors, SciPy 1.0: Fundamental Algorithms for Scientific Computing in Python, *Nature Methods* **17**, 261–272 (2020).
- [36] J. Bradbury, R. Frostig, P. Hawkins, M. J. Johnson, C. Leary, D. Maclaurin, G. Necula, A. Paszke, J. VanderPlas, S. Wanderman-Milne, and Q. Zhang, *JAX: composable transformations of Python+NumPy programs* (2018).
- [37] D. P. Kingma and J. Ba, Adam: A method for stochastic optimization (2017), [arXiv:1412.6980 \[cs.LG\]](https://arxiv.org/abs/1412.6980).